Investigation and Comparison of Cohesive Zone Models for Simulation of Crack Propagation

Sara Eliasson and Alexander Lundberg

2015-01-13

1 Abstract

Looking at crack propagation modeling today there are a few different methods that enables the possibility to simulate an advancing crack. One of these methods are cohesive zones. Cohesive zones are modeled as an interface between two continuum surfaces and are described by a constitutive law that is to represent the crack propagation.

The work carried out in this paper is supposed to give a deeper knowledge and a better understanding of the cohesive zone model to be able to further implement this method within a larger problem.

The first step is looking into linear elastic fracture mechanics to understand the theory behind cohesive zones. Understanding the theory and trying to implement it by using different traction-separation laws proposed by different authors, several difficulties were encountered. The commercial FEM-program used to implement cohesive zones, ABAQUS CAE, gives the possibility to implement linear and exponential softening in the traction-separation law. For further implementation of the traction-separation laws presented in this paper, user-defined subroutine ought to be used.

Using a double cantilever beam the traction-separation law with a linear initial loading and a linear or exponential softening is implemented in ABAQUS CAE. Controlling the penalty stiffness, the maximum traction and the fracture energy or the fracture displacement several results were produced and compared.

Looking at the results, when using the same variables for the exponential and linear softening, there is no big difference in the results of the behavior of the beam. The curves for both implementations coincide very well. There are differences in the convergence of the calculations, both methods converge well but the linear softening not as well as the exponential softening. When looking at different variables that vary fracture energy and maximum traction, the traction-separation law and the beam is behaving very well according to theory.

An explanation of the cohesive zone model and how it can be implemented it is proposed. There is no new theory presented, only a summary of various different theories developed by other authors. With the knowledge gathered throughout this project it is not possible to apply the theory of cohesive zones on more advanced problems. The next step in the process will be to examine phase transformation in steel in an advancing crack.

2 Preface

This report is a bachelor thesis written at the Solid Mechanics Department at LTH. When working with another topic where cohesive zones were proposed as a method suitable for crack propagation analysis, not much thought was given to the complexity of the cohesive zones. When it was clear that more information was needed regarding these so called cohesive zones to get an understanding of what was happening and why, it was chosen to pursue a new problem formulation before continuing on with the other issue.

We want to thank Håkan Hallberg, our supervisor, for the great support he has given and for the commitment he has shown. We also want to thank Mathias Wallin, our examiner, and the people at the Solid Mechanics Department for helping us out when we encountered different problems and for showing such a big interest in our work.

2.1 Individual Contributions

Working with the report both Alexander Lundberg and Sara Eliasson has tried to distribute the work evenly among them. They have collaborated, trying to discuss problems and make sure both have equal knowledge about the problem formulation. Both find it important that they can answer questions that may rise.

To make the work easier and to make sure one doesn't miss anything, Sara has had the main responsibility for the report and Alexander the main responsibility that the correct results are produced.

2.2 Ethnical considerations

Ethnical aspects are not relevant to the subject at hand.

Contents

3 Introduction

The information given to the reader in this report is supposed to help to get a better understanding about what a cohesive zone is and what it is useful for. Why do we use cohesive zones? Why is the choice of parameters so important to make the calculation run smoothly? How do we model them in a FE-calculation?

The goal with the report is to be able to answer the questions above and to be able to use all information gathered and implement the cohesive zone model in other problem formulations. The work is also intended to be an aid in choosing a suitable traction-separation formulation for a specific problem given.

The report is limited to a discussion and review on cohesive zones. No basic Finite Element (FE) theory will be given. It is assumed that the reader already has understanding and basic knowledge in this area. The calculations made in ABAQUS will not be explained from a FE perspective except for the cohesive elements.

Another limitation are the analytical results. It would provide additional value to have a comparison with an analytical solution. But the time limit prevented us from doing a good analytical solution worth comparing the numerical results to. The calculations that should have been done for this require more literature study in another area. This might be something to consider in future work.

4 Method

Looking into cohesive zones there is at first a lot of information to be found in the literature. Before starting to model a cohesive zone the theoretical aspects of cohesive zones are studied. At first understanding is built on why we use cohesive zones and then also understanding on how they work. Learning more and getting a better understanding is pivotal before implementing it in the FE-program. So the first step is to find useful information about cohesive zones in articles and books.

Modeling of the cohesive zones is done in a commercial FEM-program called ABAQUS CAE. ABAQUS is a very powerful tool for FE-calculations. ABAQUS gives the opportunity to use user-defined subroutines which makes it possible to write your own calculation or specifications for the cohesive zone in, for example, FORTRAN code. This is not used for this report, instead functionality already available in the software was used to investigate the possibilities and limitations of ABAQUS.

As a point of departure, the ABAQUS manual [30] was used to learn more about how the cohesive elements was modeled in the software. Gradually, making the models more advanced, it was possible to create a model that was suitable for this report.

Cohesive zones are for most parts implemented in fracture analyses and used to simulate crack growth. For this report the cohesive zones are used for studying crack tip conditions at a mode I crack. Crack modes are discussed further in section 5. For the crack tip it is assumed that the nonlinear effects are confined to a very small region around the crack tip. This makes it still possible to use linear elastic theory for the calculations of the crack [18].

A single numerical model of a double cantilever beam is used to gather simulation results in a consistent way. Model variations are also studied, for example, in terms of varying mesh density in the cohesive zone and by using different so-called traction-separation laws to describe the cohesive behavior. These aspects are discussed further in subsequent sections.

5 Linear Elastic Fracture Mechanics

There are three different types of pure crack modes, see figure 1. Mode I is when the loading is applied normal to the crack plane and tends to open the crack. Mode II is in-plane shear loading and tends to slide the crack faces over each other. Mode III is out-of-plane shear, as seen in figure 1 the crack edges are moved across each other in opposite directions [2]. Also mixed modes may occur as combinations of any of the three basic modes.

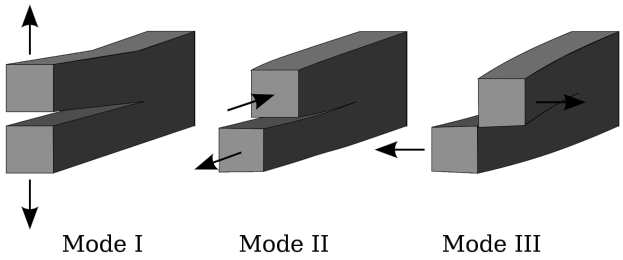

Figure 1: Illustration of the three different crack modes, taken from [1].

Early work in the field of fracture mechanics regarding stress concentrations around elliptical holes was developed by C.E. Inglis in 1913 [12]. His theory predicted that the stresses at a perfectly sharp crack tip approach infinity. In other words; that the material would have zero strength [20]. Instead of analysing the stress state in the vicinity of the crack tip, A.A. Griffith developed a theory based on energy-balance [9].

The energy criterion is based on the principle that crack extension can only occur when the energy available for crack growth is sufficient to overcome the resistance of the material. This resistance includes all types of energy dissipation related to crack extension, for example surface energy and plastic work [2].

The early work by Griffith was later developed further by G.R. Irwin[13]. Irwin defined the energy release rate, G, as the rate of change in potential energy with crack area for a linear elastic material. Crack extension occurs when the energy release rate reaches a critical value, $G = G_c$, which is a measure of fracture toughness.

On the atomic scale, fracture occurs when the applied stress and work are sufficient to sever the atomic bonds. The bond between atoms is caused by the attractive electrostatic force between opposite charges. The cohesive strength can be derived in terms of the cohesive stress. This is shown in figure 2 and

provides the theoretical strength as

$$\sigma_c \approx \frac{E}{\pi} \tag{5.1}$$

Experiments have, however, shown that the actual fracture strength is several orders of magnitude lower than the theoretical value. This discrepancy is related to stress concentrations around flaws in the material which magnify the stresses locally.

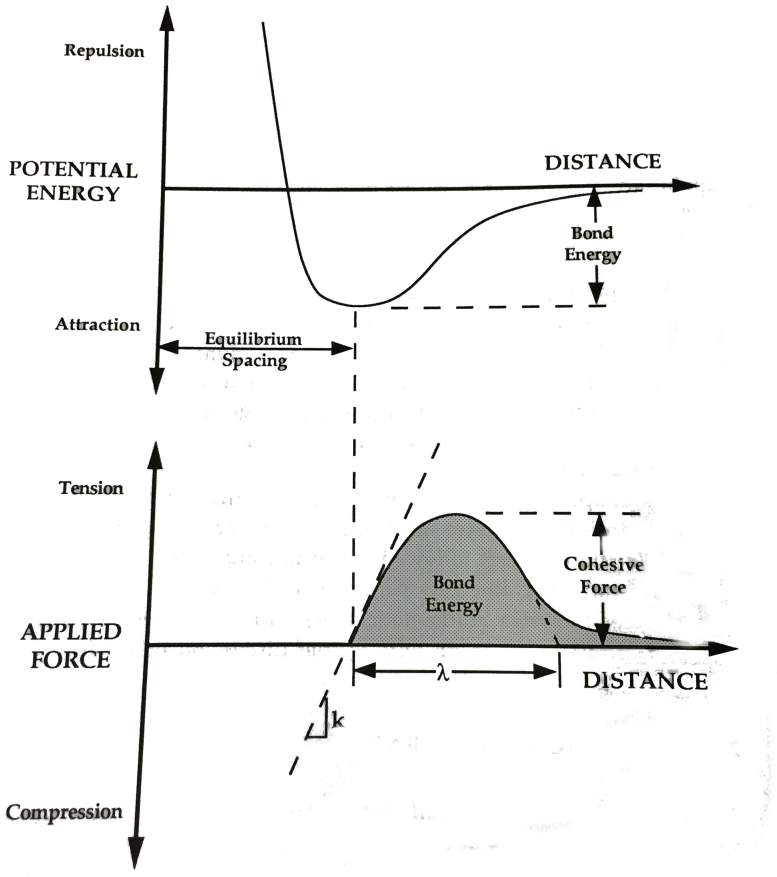

Figure 2: Potential energy and force as a function of atomic separation, taken from [2].

Griffith's energy balance is based on the first law of thermodynamics which states that a system that goes from a state of nonequilibrium to a state of equilibrium will have a net drecrease in energy. The interpretation of the application on cracks is that a crack can only grow if the fracture process results

in constant or decreased total energy [9]. Hence, the critical condition for crack extension can be defined as the point where crack growth occurs under equilibrium conditions, with zero net change in total energy [2]. The balance equation under equilibrium conditions for an incremental increase in crack area, dA, can therefore be expressed as

$$\frac{dE}{dA} = \frac{d\Pi}{dA} + \frac{dW_s}{dA} = 0 \tag{5.2}$$

which is equivalent to

$$-\frac{d\Pi}{dA} = \frac{dW_s}{dA}$$

where E is the total energy, W_s is the work needed to create two new surfaces and Π is the potential energy in the form of strain energy and work done by external forces. For an edge crack, two new surfaces are created when a crack is formed. Thus the expression for W_s takes the form

$$\frac{dW_s}{dA} = 2\gamma_s \tag{5.3}$$

where γ_s is the material specific surface energy.

Griffith first developed his theory while investigating cracks in glass. It has since been shown that his equation is valid for ideally brittle solids. The theory does, however, greatly underestimate the fracture strength of ductile materials such as metals. A modification to Griffith's approach was later developed by Irwin and Orowan [20]. The modified version of the energy-balance equation accounts for plastic flow. In brittle materials cracks form simply by breaking the atomic bonds, and the surface energy represents the total energy of the broken bonds in a unit area. Crack propagation in ductile metals, on the other hand, include a plastic zone in the vicinity of the crack tip. In this plastic region dislocation motion occurs. The process of plastic flow around the crack tip contributes to additional energy dissipation. The modified expression takes the form

$$W_f = \gamma_s + \gamma_p \tag{5.4}$$

where γ_p is the plastic work per unit area of surface created. It has been shown that fracture in ductile metals under highly plastic conditions involve dissipation mostly due to plastic work, rather than separation. In other words γ_s is small compared to γ_p as discussed by Siegmund and Brocks, cf. [24].

Irwin later developed an energy criterion for fracture that is, in essence, equivalent to Griffiths criterion. The concept is based on the energy release rate, G,

defined as a measure of energy available for an increment of crack extension [2]

$$G = -\frac{d\Pi}{dA} \tag{5.5}$$

Crack extension occurs when the energy release rate reaches a critical value, i.e when

$$G = G_c = \frac{dW_s}{dA} = 2W_f \tag{5.6}$$

Important to note is that these theories are derived under the assumption that the material response is strictly linear elastic. This means that inaccurate results may be produced when applying the model on nonlinear problems. The criterion for this theory to be valid is that the global behavior of the structure must be linear elastic, while plasticity must be confined to small regions around the crack tip [2].

6 Cohesive Zone Modeling of Fracture

Failure and fracture is a big part of many fields in engineering. It is therefore important to understand and to be able to do calculations on failure processes and fractures. To analyze these phenomena efficiently in arbitrary geometries, a general numerical method is needed that can describe the initiation and evolution of a crack. The method should include and be able to simulate the initial loading, the damage initiation with initial debonding, and the damage evolution until complete separation and failure has occurred. A method used for these kind of problems is modeling with cohesive zones. Cohesive zone models have been proved useful in many different varieties of fracture issues in homogeneous solids as well as in analyzing interface crack problems.

For this report a cohesive zone model will be used to analyze crack propagation. For the analysis a numerical FE model will be implemented. The cohesive zone is defined as an interface in between the structure faces where the crack advance will take place. The interface consists of cohesive elements which are set to behave in the same way as a crack would when it propagates. So for a cohesive zone model no elements but the cohesive elements are damaged. The crack will only propagate where cohesive elements are modeled. This requires a pre-defined crack path.

Cohesive zone models are based on theory from Barenblatt and Dugdale [3, 8]. Their method for using cohesive zones to represent a crack propagation path is very similar to Griffith's theory based on a surface energy that measures the resistance against crack advance.

Barenblatt and Dugdale's theory on cohesive zones is based on a method trying to explain how a crack advances. The cohesive zone is formulated to imitate the behavior ahead of the crack tip. Both Barenblatt and Dugdale divide the crack surfaces into two separate regions, one part that is stress free and another part which is loaded by cohesive stresses. Dugdale assumed that there is a plastic zone near the crack tip. Within this plastic zone there is a stress acting across the crack that is equal to the yield strength, σ_γ. Dugdale examined the yielding of steel sheets and investigated yielding in the sheets at the end of slits. He obtained a relation between plastic yielding and external applied load and found that the influence of yielding was approximately represented by a long crack extending into the region that had a stress equal to the yield stress. Dugdale's theory holds for plane stress but the crack opening stresses can be greater than the equivalent stress in a multiaxial stress state.

Barenblatt investigated brittle materials and instead of a constant stress in the cohesive zone he let the stress vary with deformation in the zone ahead of the crack tip. The stress of the cohesive zones works as a restraining stress that keeps the separating surfaces together. It corresponds to atomic or molecular attractions. The restraining stress, the stress in the cohesive zone, can be seen as a function of the separation distance, $\sigma = \sigma(\delta)$, see figure 3.

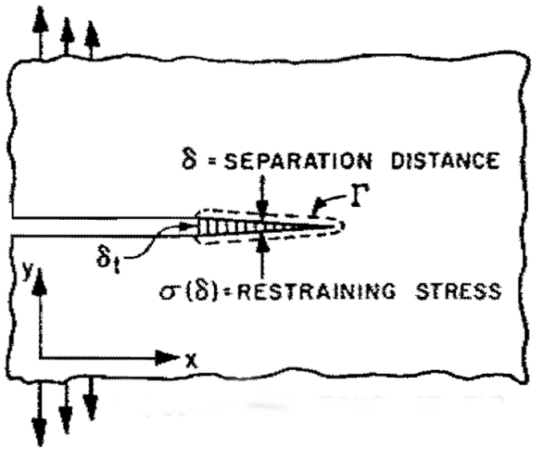

Figure 3: The cohesive zone ahead of a crack tip, taken from [3].

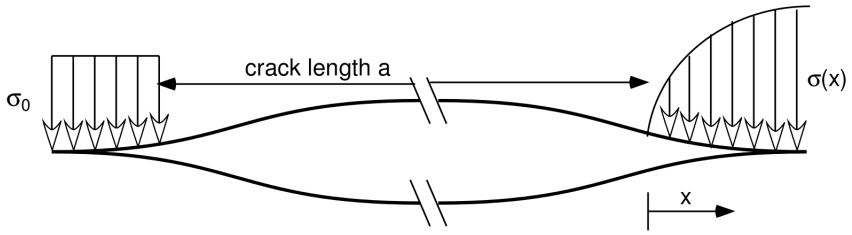

Figure 4: To the left is Dugdale's crack model and to the right is Barenblatt's crack model showing the separation of a crack connected by a cohesive interface, taken from [4].

In figure 4 it is seen in each end of a crack the difference between Dugdale's and Barenblatt's theories. Looking at the right end we see Barenblatt's crack model where the cohesive stress varies with the crack tip displacement. To the left we se Dugdale's crack model where the cohesive zone has a constant stress equal to the yield stress.

When using cohesive elements a constitutive equation describes the behavior of the failing cohesive material elements in front of the crack tip. The constitutive relation for a cohesive interface is such that the traction across the interface will vary depending on the separation of the crack. With increasing separation, the traction will reach a maximum, start to decrease and eventually be reduced to zero. When the traction is zero a complete decohesion is allowed. A typical cohesive stress-displacement diagram is shown in figure 5. The constitutive behavior of the cohesive elements is described by a traction-separation law. The parameters that set the properties of the cohesive zone is the cohesive strength (a peak stress required for separation) and a cohesive energy (separation work

per unit area) [25, 27]. The traction-separation laws will be discussed in greater detail in the next section.

Looking at figure 3, Γ represents the contour tracing an arbitrary path surrounding the crack tip, and δ_t is the separation distance at the crack tip. To connect cohesive theory with Griffith's work we evaluate the J-integral for the cohesive zone as

$$J = \int_{\Gamma} (W \mathrm{d}y - \mathbf{T} \frac{\partial \mathbf{u}}{\partial x} \mathrm{d}s) \tag{6.1}$$

Looking at only the cohesive zone, using path independence and shrinking the contour Γ down to the lower and upper surface of the cohesive zone, this results in $dy = 0$ on Γ. The J-integral then becomes

$$J = -\int_{CZ} \sigma(\delta) \frac{\mathrm{d}\delta}{\mathrm{d}x} \mathrm{d}x = -\int_{CZ} \frac{\mathrm{d}}{\mathrm{d}x} \left\{ \int_0^{\delta} \sigma(\delta) \mathrm{d}\delta \right\} \mathrm{d}x = \int_0^{\delta_t} \sigma(\delta) \mathrm{d}\delta \tag{6.2}$$

When a cracked structure is exposed to some external loads the crack surfaces are subjected to forces which restrain the surfaces from separating. These forces can be seen as cohesive forces. The cohesive stress is a function of the relative displacement between the crack surfaces, $\sigma = \sigma(\delta)$. The external loads will increase δ until it reaches δ^*, see figure 5. When δ^* is reached the bond between the crack faces breaks and new free surfaces are created.

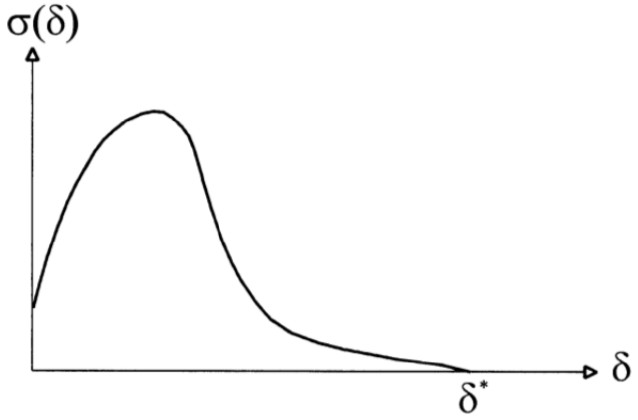

Figure 5: A typical stress-displacement diagram for a cohesive element, taken from [5].

When two new free surfaces are created, the atoms can be considered to be pulled apart. They are slowly moving out of range from their neighbours. For

the process where new free surfaces are created, the cohesive stresses perform some amount of work. The work is written as

$$W = \int_0^{\delta^*} \sigma(\delta) \mathrm{d}\delta \tag{6.3}$$

According to equation (6.2) this relation is equal to the J-integral. To propagate a crack through the distance Δa, a surface energy is needed which corresponds to

$$\Delta U_s = \int_0^{\Delta a} \int_0^{\delta^*} \sigma(\delta) \mathrm{d}\delta \mathrm{d}x = \Delta a \int_0^{\delta^*} \sigma(\delta) \mathrm{d}\delta \tag{6.4}$$

The area under the traction-separation curve is by definition twice the surface energy. Recalling equation (5.3), γ_s is the surface energy for one new free surface created and for a crack we have two new free surfaces. This gives us

$$\int_0^{\delta^*} \sigma(\delta) \mathrm{d}\delta = 2\gamma_s + \gamma_p \tag{6.5}$$

If the cohesive zone is negligible in size compared to the characteristic lengths of the structure around the crack it can be concluded that Griffiths theory and the theory of atomic cohesive forces are identical, cf. equation (5.3).

The information above on cohesive zone models is collected from several authors, see references [1, 8, 15, 17, 19, 21, 29]

6.1 Traction-Separation Laws

The cohesive elements are initially made of a damage-free bulk material which will eventually describe the damage and failure of the structure. The damage behavior is typically described by a traction-separation law, as discussed in the previous section, also cf. [22].

Depending on the material, one has to choose a suitable traction-separation law which correctly describes the fracture behavior of the particular material. The cohesive elements model the initial loading, the damage initiation and the damage evolution. These three parts can be identified in a curve for the traction-separation law [30].

A basic bilinear traction-separation law, frequently used in calculations, can be seen in figure 6, where the softening after damage initiation is linear. Another

model frequently used is the one seen in figure 7, where the softening after damage initiation is described by an exponential function. Crack propagation can be simulated using different parameters that control the advance of the crack front for cohesive zone models. It can be based on either the local energy release or on the separation of the crack surfaces which corresponds to the displacement of the cohesive elements [4].

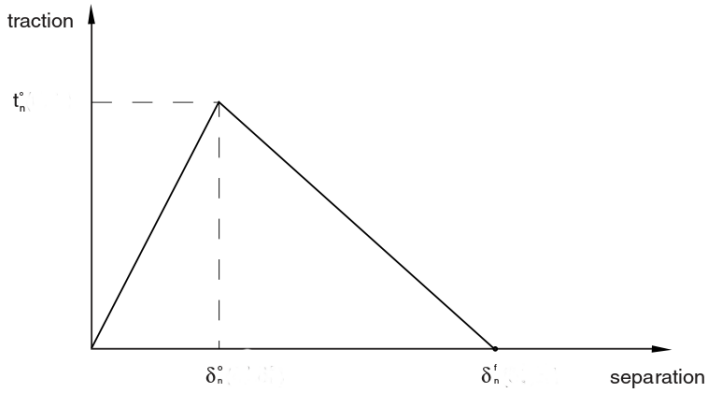

Figure 6: Illustration of a simple bilinear traction-separation law, taken from [6].

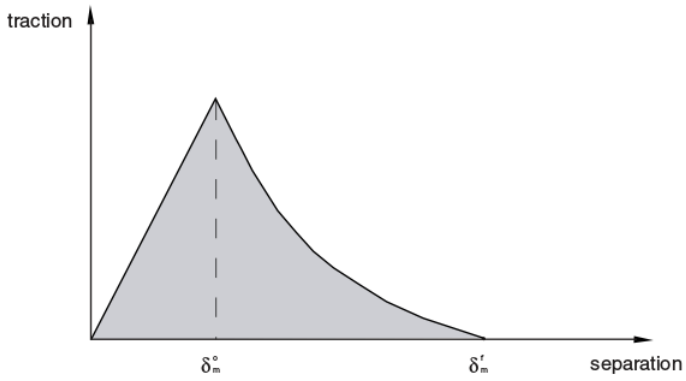

Figure 7: Illustration of exponential damage evolution in a traction-separation law, taken from [7].

The bilinear model is uniquely defined by the set of parameters that describes the top point, (δ_n^0, t_n^0), and the end point, $(\delta_n^t, 0)$, of the triangle. For both the bilinear and the exponential model the maximum traction sustainable by the cohesive element, t_n, is required. This threshold value is important since it governs when initiation of damage occurs. The penalty stiffness, K_0, is also

an important parameter in ensuring realisitic pre-crack conditions. K_0 is the slope of the first part of the curve seen in figure 6 and 7. If the penalty stiffness is insufficient, large displacements will occur in the interface, which alters the behavior of the structure.

The second part of the curve is related to damage evolution. When assumed to be linear, it can be defined by either prescribing a failure displacement, δ_n^f, or the critical energy release rate, Γ_0. When the damage evolution is assumed to be exponential the curve can be defined by prescribing a failure displacement, δ_n^f, and a exponential law parameter to define the flexion of the curve. It can also be based on the energy, Γ_0. When choosing to prescribe failure displacement, the critical energy release rate can be calculated as the area under the curve, and vice versa.

$$\Gamma_0 = \int_0^{\delta_0} T(\delta) \mathrm{d}\delta \tag{6.6}$$

When modeling fracture in ductile materials, such as steel, the deformation process involves the processes of elasticity, plasticity and damage. This means that the shape of the traction-separation law cannot easily be determined experimentally, and would have to be assumed [22]. The cohesive model is a phenomenological model. The cohesive model does not model the real physical fracture process and there is no evidence for which traction-separation law is the right one to use. In the literature there are several different approaches found.

Since there are many different assumptions of the traction-separation law a few will be described with reference to the authors. They all build on the same fundamental ideas, but include a few differences.

6.1.1 Tvergaard and Hutchinson

Tvergaard and Hutchinson developed a model for an idealized traction-separation law specified on the crack plane to characterize the fracture process in 1992 [27]. The relation can be seen in figure 8. The relation is built on an increase of traction in the cohesive element until it reaches the peak traction, $\hat{\sigma}$, at δ_1. The traction will stay the same for further separation until δ_2 is reached. Then damage evolution is modeled until reaching δ_c where fracture occurs.

The energy disspated by the cohesive elements at failure is defined by the area underneath the curve. For this specific curve, the expression for the work of separation per unit area in equation (6.6) takes the following form

$$\Gamma_0 = \int_0^{\delta_1} \sigma \mathrm{d}\delta = \frac{1}{2}\hat{\sigma}[\delta_c + \delta_2 - \delta_1] \tag{6.7}$$

To fully specify Tvergaard and Hutchinsons separation law the parameters needed to describe the fracture process are the work of separation per unit area, Γ_0, and the peak traction, $\hat{\sigma}$. Shape parameters are $\frac{\delta_1}{\delta_c}$ and $\frac{\delta_2}{\delta_c}$ [27]. We also need a set of parameters to describe the continuum behavior of the solid. The elastic-plastic solid is characterized by the following expression

$$\epsilon = \begin{cases} \sigma/E & \sigma \leq \sigma_y \\ (\sigma_y/E)(\sigma/\sigma_y)^{\frac{1}{N}} & \sigma \geq \sigma_y \end{cases} \tag{6.8}$$

The solid is specified by its Young's modulus, E, the Poisson's ratio, ν, the initial tensile yield stress, σ_y, and the strain hardening exponent, N.

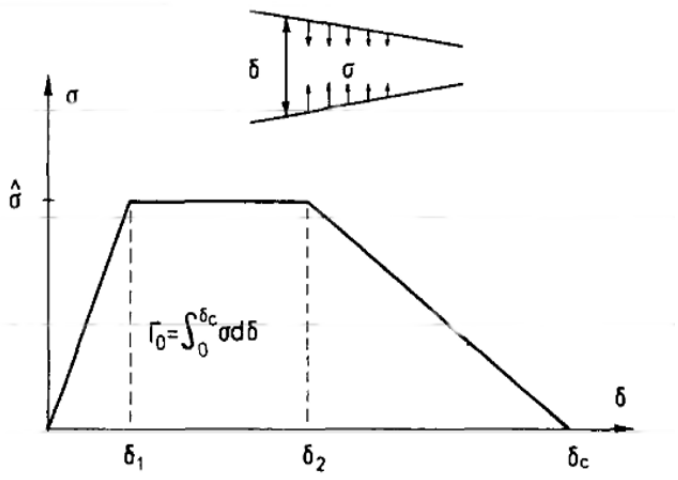

Figure 8: Graphical illustration of Tvergaard and Hutchinsons traction-separation law, taken from [8].

Tvergaard and Hutchinsons suggestion is shown mostly to be suitable for ductile fracture.

6.1.2 Needleman

A cohesive zone model which takes finite geometry changes into account proposed by Needleman [16], is used to provide a description of the behavior of void nucleation. The model is aimed to describe the evolution from initial debonding through to complete decohesion which refers to subsequent void growth in a material. The decohesion occurring can occur either in a brittle or ductile manner. This is dependent on the ratio of a characteristic length to the inclusion radius. The characteristic length is introduced by the dimensions of the surrounding material e.g. dimensions around a crack tip.

The characteristic length that is introduced comes from the fact that the model is to take finite geometry changes into account. The mechanical response of the interface is based on both a critical interfacial strength and the work of separation per unit area. Based on this, the characteristic length is introduced.

The interfacial traction is only dependent on the displacement difference across the interface. Consider two points A and B, placed on opposite sides of the interface. The interfacial traction is then seen as dependent on the displacement difference, $\Delta\mathbf{u}_{AB}$, between the points. For each point of the interface Needleman defined

$$u_n = \mathbf{n} \cdot \Delta\mathbf{u}_{AB}, \quad u_t = \mathbf{t} \cdot \Delta\mathbf{u}_{AB}, \quad u_b = \mathbf{b} \cdot \Delta\mathbf{u}_{AB} \tag{6.9}$$

and

$$T_n = \mathbf{n} \cdot \mathbf{T}, \quad T_t = \mathbf{t} \cdot \mathbf{T}, \quad T_b = \mathbf{b} \cdot \mathbf{T} \tag{6.10}$$

For the equations (6.9) and (6.10), $\mathbf{n}$, $\mathbf{t}$, $\mathbf{b}$ form a right-handed coordinate system where u_n represents the interfacial separation. A positive u_n corresponds to increasing separation and a negative u_n corresponds to decreasing separation. The constitutive relation for the mechanical response of the interface gives a dependence of the tractions (T_n, T_t, T_b) on the separations (u_n, u_t, u_b). The response can be specified as a potential $\phi(u_n, u_t, u_b)$, being defined as

$$\phi(u_n, u_t, u_b) = -\int_0^u [T_n du_n + T_t du_t + T_b du_b] \tag{6.11}$$

Needleman's model resembles the other traction-separation laws in the way that with increasing separation of the interfaces, the traction reaches a maximum value, then start to decrease to eventually vanish. When the interfacial traction has vanished complete decohesion occurs. The specific potential function that is used is the following

$$\begin{aligned}\phi(u_n, u_t, u_b) = \\ &\frac{27}{4}\sigma_{max}\delta\left\{\frac{1}{2}\left(\frac{u_n}{\delta}\right)^2\left[1 - \frac{4}{3}\left(\frac{u_n}{\delta}\right) + \frac{1}{2}\left(\frac{u_n}{\delta}\right)^2\right]\right. \\ &+ \frac{1}{2}\alpha\left(\frac{u_t}{\delta}\right)^2\left[1 - 2\left(\frac{u_n}{\delta}\right) + \left(\frac{u_n}{\delta}\right)^2\right] \\ &\left.+ \frac{1}{2}\alpha\left(\frac{u_b}{\delta}\right)^2\left[1 - 2\left(\frac{u_n}{\delta}\right) + \left(\frac{u_n}{\delta}\right)^2\right]\right\}\end{aligned} \tag{6.12}$$

The interface is undergoing a purely normal separation, $u_t \equiv u_b \equiv 0$, δ is the characteristic length and α specifies the ratio of shear to normal stiffness of the interface. By differentiating equation (6.12) we can obtain the tractions, $\mathbf{T} = \frac{\partial \phi}{\partial \mathbf{u}}$.

$$\begin{aligned} T_n = -\frac{27}{4}\sigma_{max}\Bigg\{ \left(\frac{u_n}{\delta}\right)\left[1 - 2\left(\frac{u_n}{\delta}\right) + \left(\frac{u_n}{\delta}\right)^2\right] \\ +\alpha\left(\frac{u_t}{\delta}\right)^2\left[\left(\frac{u_n}{\delta}\right) - 1\right] + \alpha\left(\frac{u_b}{\delta}\right)^2\left[\left(\frac{u_n}{\delta}\right) - 1\right]\Bigg\} \end{aligned} \tag{6.13}$$

$$T_t = -\frac{27}{4}\sigma_{max}\left\{\alpha\left(\frac{u_b}{\delta}\right)\left[1 - 2\left(\frac{u_n}{\delta}\right) + \left(\frac{u_n}{\delta}\right)^2\right]\right\} \tag{6.14}$$

$$T_b = -\frac{27}{4}\sigma_{max}\left\{\alpha\left(\frac{u_t}{\delta}\right)\left[1 - 2\left(\frac{u_n}{\delta}\right) + \left(\frac{u_n}{\delta}\right)^2\right]\right\} \tag{6.15}$$

This is the case for when $u_n \leq \delta$ and for $u_n > \delta$ we get $T_n \equiv T_t \equiv T_b \equiv 0$. The response of the potential of equation (6.12) is shown in figure 9. Here the traction T_n is plotted as a function of u_n with $u_t \equiv u_b \equiv 0$. The work of separation is the area under the curve.

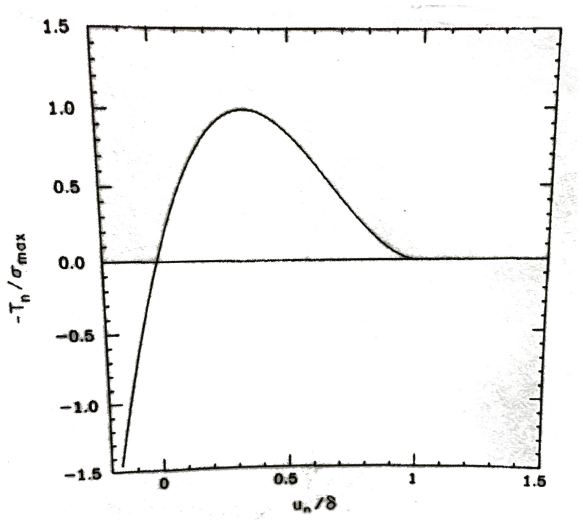

Figure 9: Normal traction across the cohesive interface as a function of the interface separation u_n with $u_t \equiv u_b \equiv 0$, taken from [9].

Needleman's interface description is a phenomenological one and is characterized by the three parameters; σ_{max}, δ and α.

6.1.3 Cornec, Scheider and Schwalbe

Cornec, Scheider and Schwalbe proposed a traction-separation law, adressing metallic materials. The method is to simulate a ductile tearing process, which consists of initiation, growth and coalescence of voids. The method used for the practical application of the cohesive model consists of a defined shape of the traction-separation law and determination of the parameters for this law [6].

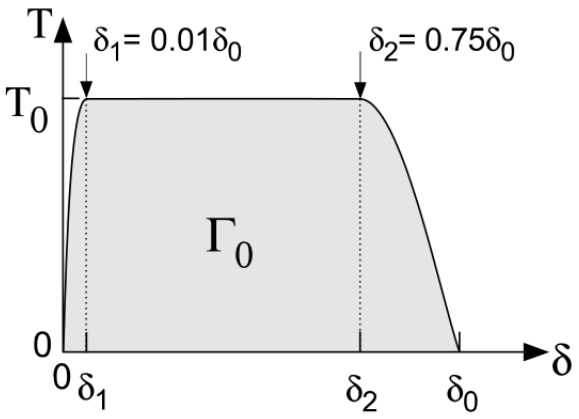

Figure 10: Graphical illustration of Cornec, Scheider and Schwalbe's traction-separation law, taken from [10].

The suggested shape function for the traction-separation law can be seen in figure 10. The three sections visible are expressed by following analytical expression

$$T = \begin{cases} T_0 \cdot \left[2\left(\frac{\delta}{\delta_1}\right) - \left(\frac{\delta}{\delta_1}\right)^2 \right] & \text{for } \delta < \delta_1 \\ T_0 & \text{for } \delta_1 \leq \delta \leq \delta_2 \\ T_0 \cdot \left[2\left(\frac{\delta-\delta_2}{\delta_0-\delta_2}\right)^3 - 3\left(\frac{\delta-\delta_2}{\delta_0-\delta_2}\right)^2 + 1 \right] & \text{for } \delta_2 \leq \delta \leq \delta_0 \end{cases} \tag{6.16}$$

With $\delta_1 = 0.01\delta_0$ and $\delta_2 = 0.75\delta_0$. The traction-separation law will be determined from three material parameters, comprising the cohesive stress, T_0, the cohesive energy, Γ_0 and the separation at material decohesion, δ_0. There are only two independent parameters since the cohesive energy can be determined from the area underneath the traction-separation curve as

$$\Gamma_0 = \int_0^{\delta_c} T \mathrm{d}\delta = T_0 \left(\frac{1}{2} - \frac{1}{3}\frac{\delta_1}{\delta_0} + \frac{1}{2}\frac{\delta_2}{\delta_0} \right) \tag{6.17}$$

Which in this particular case can be simplified to

$$\Gamma_0 = 0.87 T_0 \delta_0 \tag{6.18}$$

According to Cornec, Scheider and Schwalbe a very simple traction-separation law would be chosen just as

$$\Gamma_0 = T_0 \delta_0 \tag{6.19}$$

But the slopes are chosen to avoid sharp edges. The slope in the beginning helps out with numerical problems between the cohesive elements and the surrounding continuum elements. The slope in after δ_2 down to δ_0 models the rapid softening during void growth and coalescence.

6.1.4 Schwalbe and Cornec

Schwalbe and Cornec [23] suggested a crack growth resistance curve, at fracture, for a material constitutive model that is defined by the parameters σ_0, E, ν and n, where n is a strain hardening exponent. They also concluded that the total work to fracture can be broken down into three parts; work to separation, Γ_S, plastic energy, Γ_P and elastic energy, Γ_E. This results in a total energy on the form

$$J = \Gamma_S + \Gamma_P + \Gamma_E \tag{6.20}$$

The work of separation and the plastic energy can be allocated to the process zone and the plastic zone, see figure 11. Geometry effects are caused by the plastic energy whilst the separation work is more of a material specific variable.

In the model there are two constants representing the porosity in the material; f_0 representing the initial porosity and f_c which is the final porosity at fracture. These quantities are related to the material's microstructure. Since the microstructure of the material is a fundamental part of how the crack will advance these parameters are important and is a fundamental basis of the fracture model. Since Schwalbe and Cornec have been looking at a porous model, this is a brittle fracture process determined by void growth and coalescence.

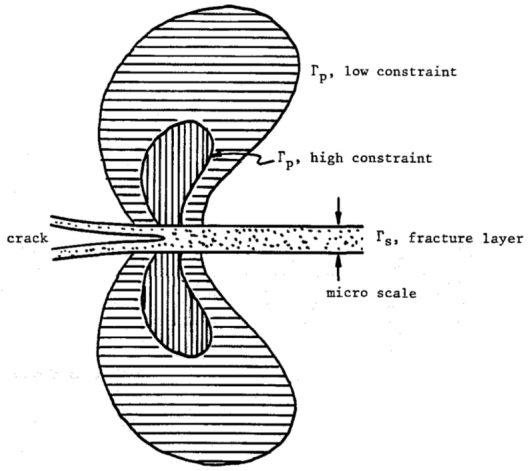

Figure 11: The process zone and the plastic zone allocating the work to fracture and the plastic energy, respectively, taken from [11].

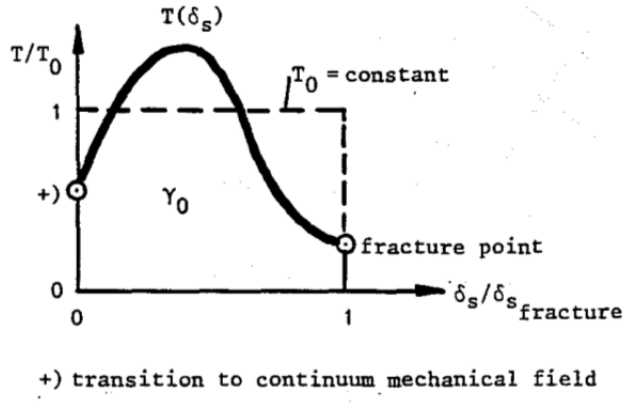

Figure 12: The traction-separation law of the cohesive zone model by Schwalbe and Cornec, taken from [12].

The cohesive zone model is based on the fact that the cohesive energy, γ_0, is constant during crack growth. The cohesive energy is presented as a material property. As in previous traction-separation laws, the energy is based on the area underneath the curve of the cohesive force law. To simplify the cohesive stress, T_0 is taken as a constant. Figure 12 illustrates how the traction-separation law of the cohesive zone model is defined.

The total work equals the cohesive energy and can be expressed as

$$J_i = \int_0^\infty T(\delta_S)\mathrm{d}\delta_S \cong T_0 \cdot \delta_{S,fracture} = \gamma_0 \tag{6.21}$$

Schwalbe and Cornec used this model to predict crack growth resistance curves for various geometries and load versus displacement relationships for structural parts.

7 Cohesive Zone Modeling in Abaqus

Different cohesive zone models can be defined in ABAQUS CAE, which is the pre- and post processor of ABAQUS. In the present study, the cohesive zone model is implemented in a double cantilever beam (DCB). A DCB is a good model to be able to investigate the basic behavior of the cohesive elements and find a traction-separation law that is suitable for predicting crack growth. DCB structures in combination with cohesive zones have been employed in, for example, [1] and [5]. For the analysis a plane stress condition is implemented for conditions of small-scale yielding where LEFM applies. Plane stress is used since we are looking at a DCB which is small in the thickness direction compared to the in-plane dimensions.

Arbitrary traction-separation laws are not easily implemented through the CAE interface. For more general formulations one needs to resort to writing user-defined subroutines.

Since the concept of user-defined subroutine will not be pursued in this report the results will be those that are possible to create by just using ABAQUS's own interface. ABAQUS provides the possibility to define the initial traction-separation stiffness, combined with linear or exponential softening during evolution of damage, cf. figure 6 and 7. The damage evolution can be defined by displacement or energy.

7.1 Cohesive Zone Element

The cohesive elements are modeled as an own separate part of the model. The cohesive layer is one element layer thick in between the regions where the crack is to advance. For two-dimensional modeling, the four-node cohesive element COH2D4 is used. The cohesive element has a linear displacement formulation and the stress in the third direction does not affect the element behavior and thus there is no difference between plane stress and plane strain condition. The separations and stresses in the cohesive elements are calculated in each increment at the integration points according to the traction-separation law. When the critical separation energy is reached, the element has failed. The integration point which contributes to the stiffness obtains the status "failed". Once a integration point has lost its stiffness, it will never obtain another status [6].

To understand the calculations done by ABAQUS it is interesting to know how the stiffness matrix of a cohesive element is formulated [21]. It can be derived from the principle of virtual work, which for the cohesive stresses is defined by

$$\delta\Pi_i = \int \mathbf{t} \cdot \delta[\mathbf{u}] \mathrm{d}A \tag{7.1}$$

Where the separation is denoted as $[\mathbf{u}]$ and t is the vector of the cohesive stresses related to the separations.

The coordinates and separations are written, using a FE approximation. The displacements $[\mathbf{u}]$ are replaced by

$$\mathbf{u} = \mathbf{V}_u \cdot \mathbf{u}_e \tag{7.2}$$

Where $\mathbf{V}_u$ is a matrix with the shapefunctions and $\mathbf{u}_e$ is the displacement for each node. $\mathbf{V}_u$ is defined as

$$V_{ij} = \begin{pmatrix} f_1 & 0 & f_2 & 0 & ... & f_n & 0 \\ 0 & f_1 & 0 & f_2 & ... & 0 & f_n \end{pmatrix} \tag{7.3}$$

Using equation (7.2) and inserting it into equation (7.1) leads to

$$\delta\Pi_i = \delta[\mathbf{u}_e] \cdot \int \mathbf{V}_u^T \cdot \mathbf{t} \mathrm{d}A \tag{7.4}$$

The cohesive stresses $\mathbf{t}$ in equation (7.1) are nonlinear functions of the displacement. This makes it impossible to extract the nodal displacement from the integral, and a linear system of equations can not be setup. This means we will need to find a tangential stiffness matrix. The tangential stiffness matrix is the change of the internal forces corresponding to infinitesimal changes in displacements [14].

To find the tangential stiffness matrix, the integral part of equation (7.4) is differentiated. The integral in this equation can be seen as the internal forces.

$$\delta\Pi_a = \delta[\mathbf{u}_e]\mathbf{f} \tag{7.5}$$

Where

$$\mathbf{f} = \int \mathbf{V}_u^T \cdot \mathbf{t} \mathrm{d}A \tag{7.6}$$

When differentiating the internal forces the total differential of the traction is used as

$$\mathrm{d}\mathbf{t} = \frac{\partial \mathbf{t}}{\partial [\mathbf{u}]} \cdot \mathrm{d}\mathbf{u} \tag{7.7}$$

For $\mathrm{d}\mathbf{u}$ the difference $\Delta\mathbf{u}$ is used. Looking at the total displacement at the time $t + \Delta t$ we get $\mathbf{u}^{t+\Delta t} = \mathbf{u}^t + \Delta\mathbf{u}$. The next step is to write the differential formulation of the integral in equation (7.4) so that we can find the tangential

stiffness matrix $\mathbf{K}$. Looking at the differential of only the integral it can be written as

$$\int \mathbf{V}_u^T \cdot d\mathbf{t} \mathrm{d}A = \int \mathbf{V}_u^T \cdot \frac{\partial \mathbf{t}}{\partial [\mathbf{u}]} \cdot \mathbf{V}_u \mathrm{d}A \cdot \Delta[\mathbf{u}_e] = \mathbf{K} \cdot \Delta[\mathbf{u}_e] \tag{7.8}$$

The integration is evaluated numerically using the Gauss integration algorithm, whereby the tangential stiffness matrix can be written as

$$\mathbf{K} = \int \mathbf{V}_u^T \cdot \frac{\partial \mathbf{t}}{\partial [\mathbf{u}]} \cdot \mathbf{V}_u \mathrm{d}A = \sum_i \left(\mathbf{V}_u^T \cdot \frac{\partial \mathbf{t}}{\partial [\mathbf{u}]} \cdot \mathbf{V}_u \right) \Big|_i \omega_i J_i \tag{7.9}$$

The weight function for the Gauss integration is ω_i, J_i is the Jacobian determinant of the cohesive element at the specific Gauss point. The Jacobian can be calcuated from the matrix

$$\mathbf{J} = \begin{pmatrix} \frac{\partial x}{\partial \varepsilon} & \frac{\partial y}{\partial \varepsilon} \\ \frac{\partial x}{\partial \eta} & \frac{\partial y}{\partial \eta} \end{pmatrix} \tag{7.10}$$

ABAQUS uses the definition for the tangent stiffness matrix shown in equation (7.9) in the FE-calculations for the cohesive zone. In ABAQUS the cohesive zone is modeled between the two potential crack faces and tied to the upper and lower face by tie-constraints, c.f figure 13 [7].

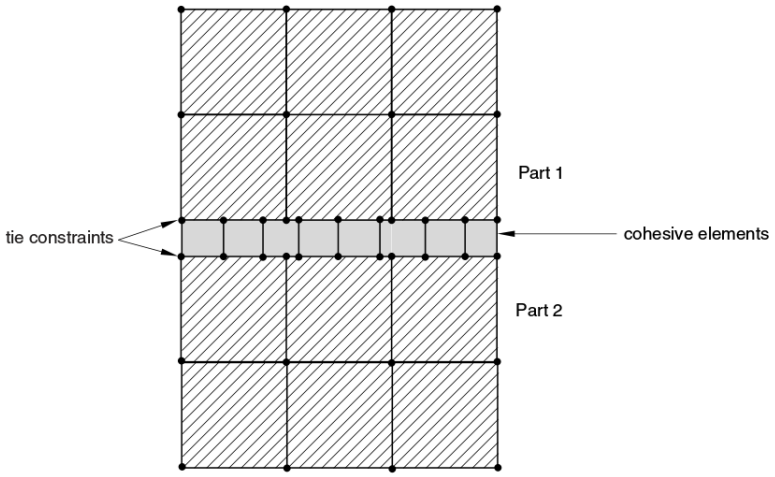

Figure 13: Illustration of the cohesive elements and how they are modeled, taken from [13].

The softening part of the cohesive law often give rise to convergence issues when running the calculations. The analysis tends to exhibit mesh sensitivity, lack of

convergence, computing inefficiency, sensitivity to element aspect ratio and so on. These difficulties need to be adressed when using cohesive zones and it is also very important to pick the right traction-separation law with the correct parameters [28].

8 Numerical Examples

Having summarized the basic theory of a cohesive zone model and traction-separation laws attention is now turned to implementation in ABAQUS. For the results a linear damage evolution and an exponential damage evolution will be compared since these are easily accessible in ABAQUS CAE without using a user-defined subroutine to describe the material behavior of the cohesive zone.

8.1 Double Cantilever Beam Model

The cohesive zone model is implemented on a double cantilever beam, see figure 14. The material properties for the beam can be seen in table 8.1. The material is linear-elastic.

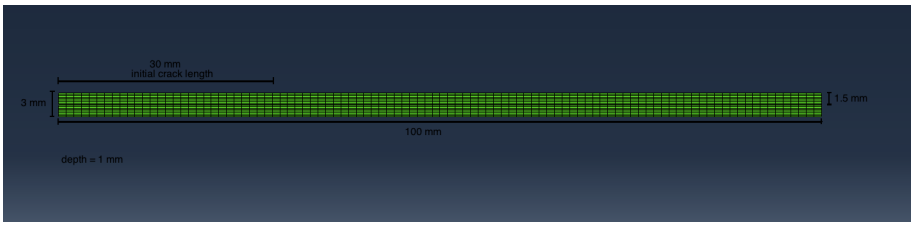

Figure 14: The abaqus model of the DCB with dimensions.

Table 8.1: Material parameters for the DCB, representative for steel.

Youngs modulus, E $[N/mm^2]$	Poission's ratio
205 000	0.3

For the DCB analysis displacement controlled loading is used. The top and bottom left nodes of the DCB are the nodes which are subjected to a vertical displacement of 8 mm in opposite directions.

Different mesh densities and element sizes are tested to find a mesh which provides an appropriate result for the beam calculation. If the mesh is too coarse true behavior will not be captured and a too fine mesh consumes unnecessary time on calculations for results that are provided also with a coarser mesh. To identify a suitable mesh disctretization, only one half of the DCB geometry is used and the simulation results are checked against the analytical expression, found from elementary beam theory, c.f [26], as

$$\delta = \frac{Pl^3}{3EI} \tag{8.1}$$

8.2 Comparison of Traction-Separation Laws

For the traction-separations laws, that are used in the cohesive zone model, to be compared in a consistent way some parameters have to be held constant. The constant parameters are the penalty stiffness, K_0, and the maximum traction, t_n. Further, it is chosen for the traction-separation laws to depend on the critical energy release rate, Γ_0, also set as a constant. In table 8.2 the values for the parameters can be seen.

Table 8.2: Parameters for the traction-separation law.

K_0	10 000	$[N/mm^3]$
t_n	100	$[N/mm^2]$
Γ_0	2	$[J/mm^2]$

When comparing the traction-separation laws for the cohesive zone a force-displacement curve will be analysed. The curve will show how the beam responds when the crack advances. By analysing the curve it is then possible to see if the choice of traction-separation law will make the crack propagation behave differently.

The mesh for the DCB is tested to find one that is possible to use for all analyses of the cohesive zone. However, the element size in the cohesive zone is also varied to investigate how the results differ with different mesh densities.

The maximum traction chosen will be used for all analyses except one where different maximum tractions are investigated to see how the results are affected.

8.3 Implementation Issues

There are two different ways to implement the cohesive behavior in ABAQUS. The first includes modeling the cohesive zone as a surface interaction. The other method, which is used in this paper, is based on implementing actual cohesive elements between the two surfaces along the crack path. The surfaces are then connected to the cohesive elements using tie constraints. These constraints tie the nodes on the slave surface, in this case the surface of the cohesive zone, to the elements of the master surface, i.e. the adjacent solid material.

When modelling the tie constraints there are different options for the discretization method. One can choose from either 'surface to surface' or 'node to surface' discretization. For this application it is important to choose the latter to ensure that all the nodes on the cohesive zone are properly connected to the ligament.

The characteristics of the traction-separation law have a great influence on the convergence. If the penalty stiffness is too high, sharp increases in stiffness will occur in elements which are suddenly loaded. Another parameter which has great influence on the convergence is the fracture energy. The fracture

energy determines, in the case of the basic triangular traction-separation law, the decrease in stiffness. As with most non-linearities, numerical issues can arise when the material softens rapidly. Lowering of the fracture energy greatly reduces the stiffness once damage is initiated and can cause convergence issues due to sharp decreases in stiffness.

Trying to implement all the traction-separation laws described in this report was very difficult. The possibility of completely defining your own traction-separation law is not accessible unless using a user-defined subroutine to define the cohesive behavior. In ABAQUS CAE it was possible to define the linear and exponential damage evolution and compare these two. For other traction-separation laws as for example Tvergaard and Hutchinson's, it is recommended to use a user subroutine to define the cohesive zone behavior.

9 Results

In this section the results from ABAQUS are presented. Running the DCB calculation with different traction-separation laws for the cohesive zone, a deformation of the beam similiar to the on seen in figure 15 should be obtained. The cohesive elements in figure 15 are seen as just black, this is because the elements are too small to distinguish. The magnified cut-out gives a closer view, see figure 16.

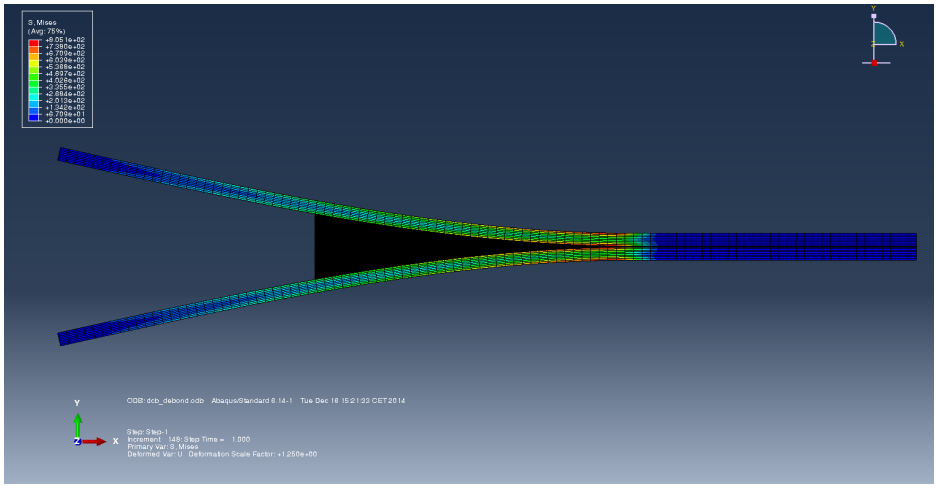

Figure 15: The deformation of the DCB after displacement controlled loading. Seen is also the deformed cohesive elements modeled inbetween the top and bottom cantilever beams.

The force-deflection curves are represented by values from the top node in the DCB which was subjected to a prescribed displacement. This node represents the behavior of the beam structure. The graphical illustrations of the traction-separation laws are constructed of values from a node in a cohesive element which is known to have collapsed.

Running the simulation in ABAQUS, a value for the damage variable can be retrieved, varying between zero and one. This variable is a good way to see when and if a cohesive element has failed. In figure 17 the red elements indicate a failed element with a damage variable equal to one.

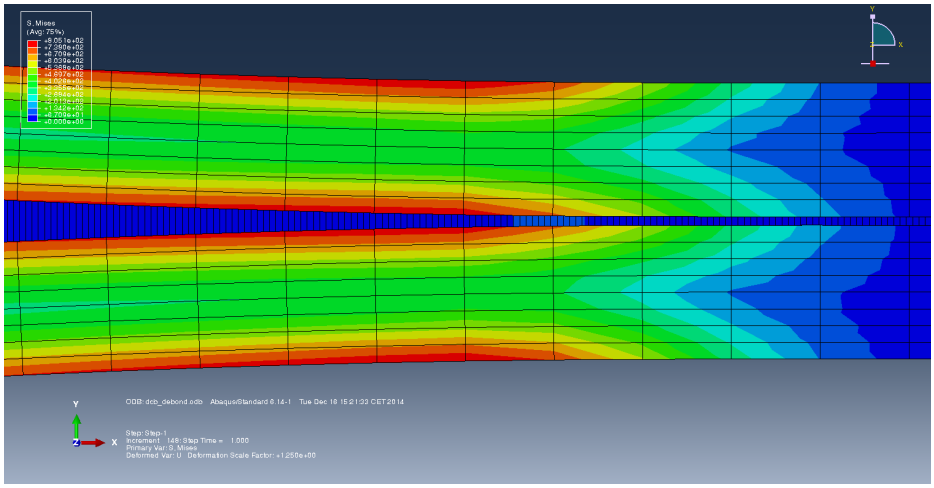

Figure 16: A magnified cut out of the DCB when deformed to get a better view of the cohesive elements. The cohesive elements are represented by the blue elements inbetween the beam parts.

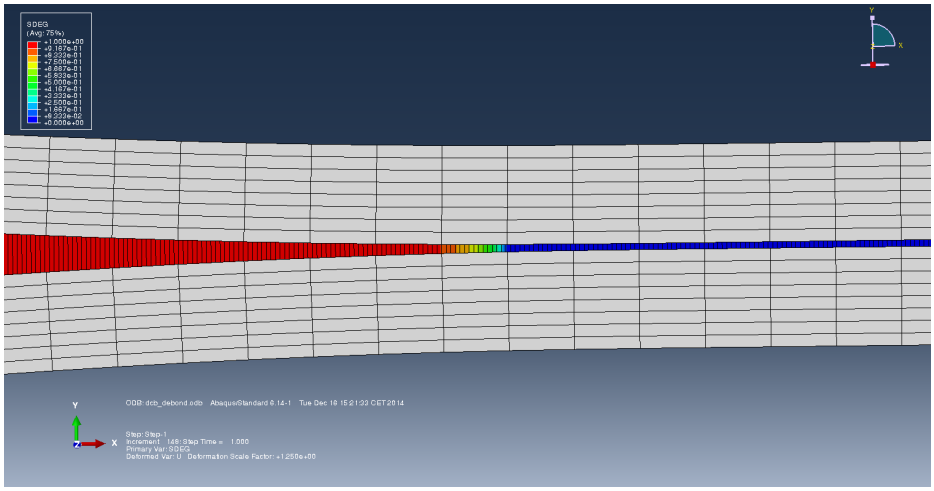

Figure 17: The damage of the cohesive elements with red indicating failure.

9.1 Choice of Mesh for the DCB

The DCB will have an unchanged mesh throughout the analyses. But the choice of the mesh is determined by analysing the convergence of the result compared to the element density. Figure 18 is showing the results of testing different element densities. The amount of elements are chosen to be 100, 400, 800 and 2400. The results obtained with different meshes are compared to the analytical

solution provided by equation (8.1).

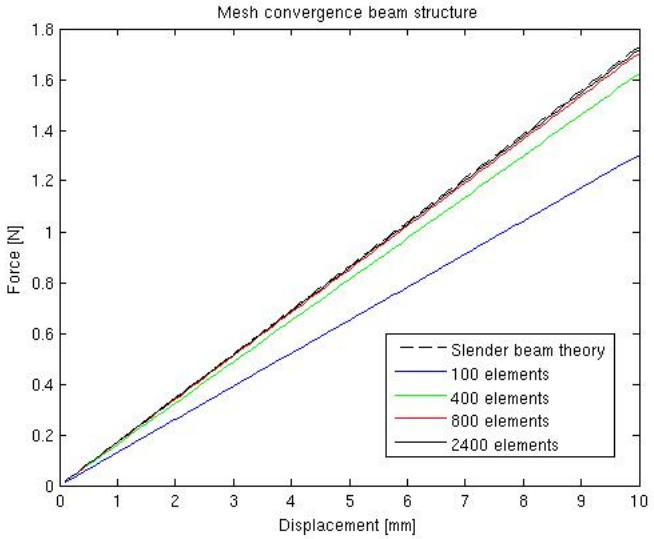

Figure 18: The element convergence for the DCB showing results provided by testing 100, 400, 800 and 2400 elements.

The final choice of mesh for the DCB came to 800 elements, 8x100.

9.2 Element Convergence for the Cohesive Zone

Looking at the influence of the mesh density of the cohesive zone on the results, three different densities were chosen. The elements for the cohesive zone is always one layer thick and was varied between 100, 300 and 500 cohesive elements. It appears as if the results are quite insensitive to the number of cohesive elements that are used.

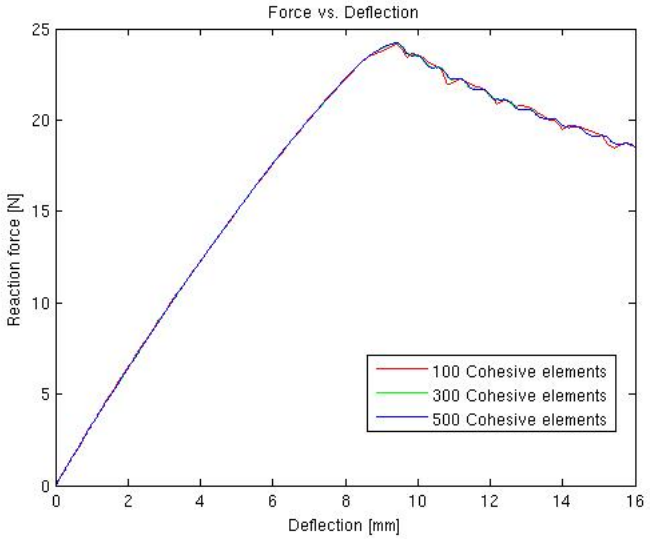

Figure 19: The element convergence for the cohesive zone showing results provided by testing 100, 300 and 500 cohesive elements.

9.3 Results for Traction-Separation Laws

Two traction-separation laws are analysed. One which is bilinear and one that is linear until damage initiation and then has a exponential damage evolution. The results are seen in figure 20, illustrated by a force-deflection curve. The traction-displacement curve for the models are shown in figure 21.

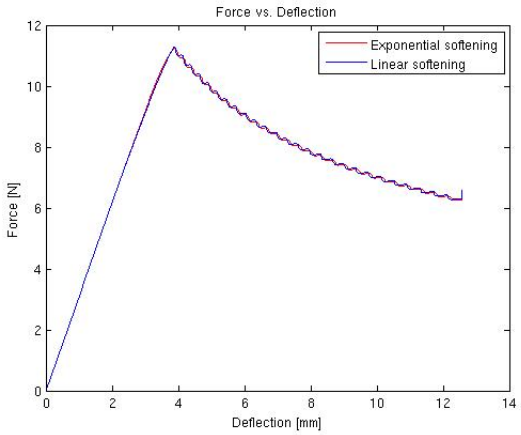

Figure 20: Showing the force-displacement curve for the linear and exponential traction-separation law.

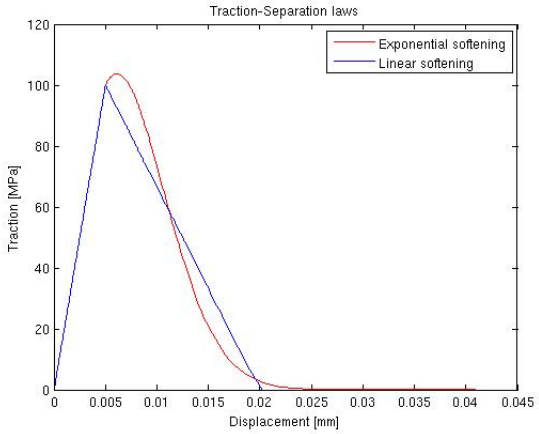

Figure 21: Showing traction-separation laws for the exponential and linear model.

Looking at figure 20, it appears as both traction-separation models provide very similar results, based on the current model set-up.

9.4 Results for Varying Fracture Energy

Seen in figures 22 and 23 are the force-deflection curve and the traction-separation curves from the simulation where the maximum traction is kept constant and the fracture energy varies. The fracture energy varies with 2, 3 and 4 J/mm^2

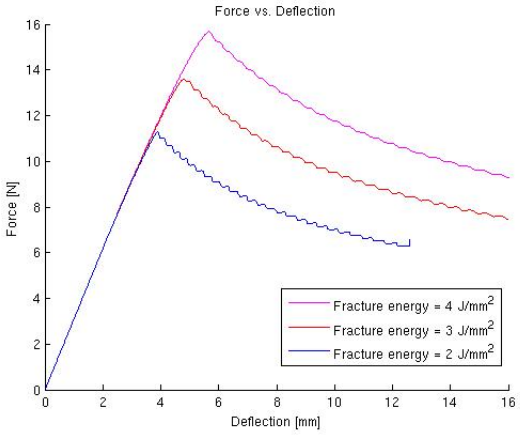

Figure 22: Force-deflection curves for the response of the DCB when varying the fracture energy.

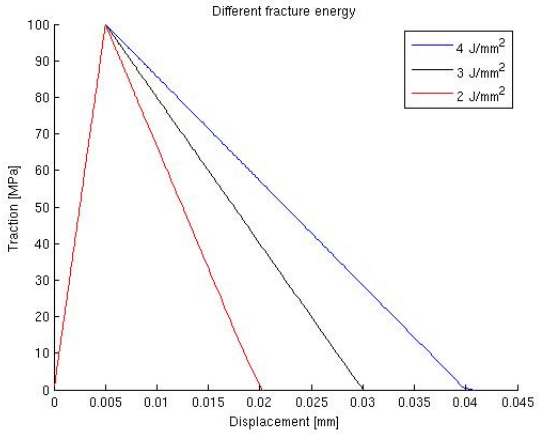

Figure 23: The traction-separation curves for a linear model when varying the fracture energy.

9.5 Results for Varying Maximum Traction

Crack propagation in the DCB model is also studied when varying the maximum traction but keeping the energy release rate constant. The resulting force-deflection curve can be seen in figure 24. The maximum traction is set as 100, 80, 50 and 10 MPa, respectively.

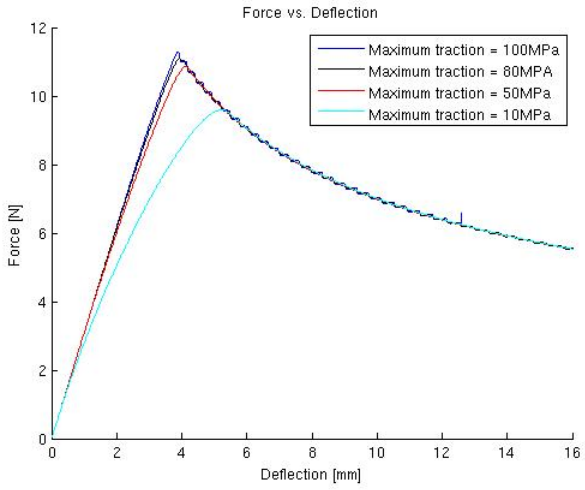

Figure 24: Showing the force-displacement curve for varying maximum traction. The maximum traction is varied between 100, 80, 50 and 10 MPa.

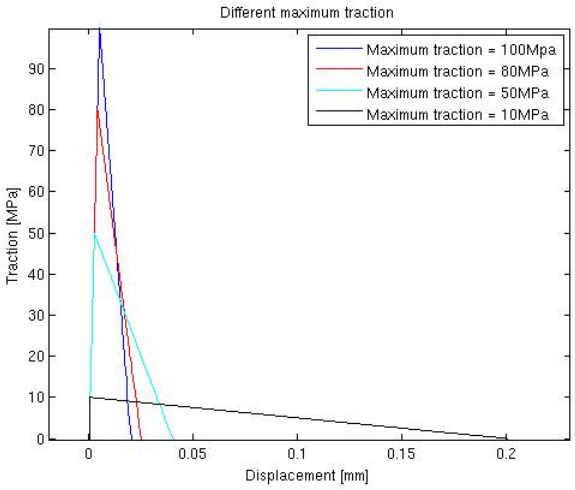

Figure 25: Showing the force-displacement curve for varying maximum traction. The maximum traction is varied between 100, 80, 50 and 10 MPa.

10 Discussion and Conclusions

The double cantilever beam is chosen to have a mesh of 8 elements across the height and 100 elements along the width. This choice comes from the fact that the amount of elements slowly converges to the result obtained with the elementary beam theory. Looking at figure 18, it is clearly seen that 100 elements is a too coarse a mesh. The result from ABAQUS with this mesh shows a huge deviation from the analytical result. Also for 400 elements the difference in the result is significant. But comparing 800 elements to the analytical result we are close enough to the correct solution to have an acceptable error. Since there is very little difference in a solution with 2400 elements and the solution with 800 elements, it is concluded that 800 elements gives a satisfying result without degrading the accuracy of the calculations.

The mesh convergence study for the cohesive zone shows that no significant difference in the results are obtained when using different mesh densities, see figure 19. The curves for the different counts of cohesive elements coincide. This shows that the number of cohesive elements will not significantly affect the results. However, the general experience from working with cohesive elements during this project is that choosing too few elements can result in instability and convergence difficulties. Using a very fine mesh in the cohesive zone can, on the other hand, lead to very long computation times. The mesh density must therefore be chosen carefully with these two points in mind.

Using an exponential softening model the calculations was perceived to converge faster. The linear softening has a good convergence as well but not as good. The behavior of the two different models does not show differences in the resulting behavior of the simulated beam. The crack extends in the same way, which is controlled by the fracture energy, and initiates at the same time, due to the choice of penalty stiffness and maximum traction. Most inequalities are seen after damage initiation which is when the damage evolution behaves according to either of the two different models. The results, however, follow the same slope and converge to about the same value.

The appearance of the traction-separation laws are seen in figure 21. There is an obvious difference between the shapes of the linear and exponential softening models. The first part of the curve, which is controlled by the penalty stiffness and the maximum traction, coincides.

The penalty stiffness is mostly set to a very high value since this choice resembles reality. If the penalty stiffness is too low, the displacement of a cohesive element will be quite large before any damage occurs. In reality a crack does not open unless the crack is advancing and damage is evolving. Since a lower penalty stiffness also greatly increases the energy absorbed by the elastic loading part of the curve it reduces the amount of energy available for the damage part of the curve for a fix fracture energy. This leads to very steep softening which, in turn, often lead to convergence difficulties. It can be concluded that a high

penalty stiffness is needed to ensure realistic pre-crack extension behavior.

The fracture energy, i.e. the area underneath the two curves in figure 21, is the same for both models. Increasing the fracture energy entails that the failure displacement is increased, since the area under the curve must increase. The damage initiation will still occur in the same place and at the same time, but the damage evolution will be a prolonged process. For the force-deflection curve in figure 20, the lowering of the stiffness in the structure is caused by damage. A higher fracture energy essentially means that more energy is needed at the crack tip to create new surfaces. Linear elastic fracture mechanics predicts that the fracture energy is proportional to the stress intensity factor squared. Since the stress intensity factor is related to the stress, it is intuitive that a higher load is needed to advance the crack. This corresponds well with the results presented in figure 22.

Looking at results from when the maximum traction is varied there is a more significant difference in the results from the beam analysis. The maximum traction varied with a constant energy implies that the failure displacement must be different. This is seen in figure 25. Since the same amount of energy is needed for the crack to advance, the crack propagation will behave in the same way. As seen in figure 24, the curves eventually coincides for all choices of maximum traction. The main thing the maximum traction affects is the pre-crack extension behavior, equal to the softening during the damage evolution.

11 Future Work

Writing this report gave us a perspective of how useful cohesive zone models can be. Even though it is not yet big in the area of crack propagation in steel it has huge potential. Most applications today are for brittle materials and very ductile materials, like polymers. The theory on the subject is endless and there are still much to look into even further. There are a lot of traction-separation models for the cohesive zone proposed by different authors and still more to come. The work on cohesive zones is a long way from being finished.

The review on the cohesive zone theory in this report can be used in many applications. Being able to use cohesive zones in FE-programs such as ABAQUS and understanding the approach makes it possible to apply the knowledge on various FE-problems involving crack growth.

A proposal on further work with crack advance is to consider Hallberg's article from 2007 [11]. In this article, a constitutive model for martensite transformation in austenitic stainless steel is derived. In a subsequent article, also by Hallberg, from 2011 [10], results are shown from a stationary crack where the martensite transformation at the crack tip is included. Using this constitutive model with a cohesive zone model on an advancing crack would make it possible to investigate how the martensite transformation influences the crack propagation.

Using a cohesive zone model for this problem one has to consider that the fracture toughness is different for the martensitic and austenitic phases. This means that the material response in the vicinity of the crack tip will change and the traction separation law will have to account for these changes. An example of possible alterations that could be made to the cohesive zone model to account for the phase transformation could be by varying fracture energy and maximum traction to account for changes in fracture toughness and yield stress.

A good idea to look into is also the comparison of the results in this report against further analytical results.

All traction-separation laws decribed in this paper were not implemented in ABAQUS. The models presented by Tvergaard and Hutchinson and Scheider and Cornec proved to be difficult to implement using ABAQUS CAE. In order to implement these models user-defined subroutines are called for. This was not done in this project due to lack of time, but it would be of great interest to do this and compare the results with the ones presented in this paper.

12 References

[1] G. Alfano, M. A. Crisfield, *Finite Element Interface Models for Delaminaion Analysis of Laminated Composites: Mechanical and Computational Issues.* 2001

[2] T.L. Andersson, *Fracture Mechanics - Fundamentals and Applications.* Department of Mechanical Engineering, Texas A&M University. CRC Press, 1991.

[3] G.I. Barenblatt, *The Mathematical Theory of Equilibrium Cracks in Brittle Fracture.* Advances in Applied Mechanics vol. 7, pp 55-129, 1962

[4] J. Chen M. Crisfield, *Predicting Progressive Delamination of Composite Material Specimens via Interface Elements.* Mechanics of Composite Materials and Structures 6:301-317, 1999

[5] M.A. Crisfield, G.A.O. Davies, H.B. Hellweg, Y. Mi, *Progressive Delamination Using Interface Elements.* Journal of Composite Materials, 1998

[6] A. Cornec, I. Scheider, K-H. Schwalbe, *On the Practical Application of the Cohesive Model.* Institute for Materials Research, GKSS Research Centre Geesthacht, 2003

[7] T. Diehl, *Modeling Surface-Bonded Structures with ABAQUS Cohesive Elements: Beam-Type Solutions.*

[8] D.S. Dugdale, *Yielding of Steel Sheets Containing Slits*, Engineering Department, Univeristy College ov Swansea, 1959

[9] A.A.Griffith, *The Phenomena of Rupture and Flow in Solids.* 1920

[10] H. Hallberg, L. Bank-Sills, M. Ristinmaa, *Crack Tip Transformation Zones in Austenitic Stainless Steel.* Division of Solid Mechanics, Lund University, 2011

[11] H. Hallberg, P. Håkansson, M. Ristinmaa, *A Consitutive Model for the Formation of Martensite in Austenitic Steels under Large Strain Plasticity.* Division of Solid Mechanics, Lund University, 2007

[12] C.E Inglis, *Stresses In a Plate Due to the Presence of Cracks and Sharp Corners.* Cambridge, 1913

[13] G.R Irwin, *Analysis of Stresses and Strains Near the End of a Crack Traversing a Plate.* Journal of Applied Mechanics 24, 361–364, 1957

[14] S. Krenk, *Non-Linear Modeling and Analysis of Solids and Structures.* Cambridge University Press, 2009

[15] N. Moës, T. Belytschko, *Extended Finite Element Method for Cohesive Crack Growth.* Department of Mechanical Engineering, Northwestern University, USA, 2001

[16] A. Needleman, *A Continuum Model for Void Nucleation by Inclusion Debonding.* Division of Engineering, Brown University, 1987

[17] A. Needleman, *An Analysis of Decohesion Along an Imperfect Interface* - 1988. International Journal of Fracture vol.42 pp.21-40, 1990

[18] F. Nilsson, *Fracture Mechanics - From theory to applications.* Royal Institute of Technology, 2001

[19] J.R. Rice, *A Path Independent Integral and the Approximate Analysis of Strain Concentration by Notches and Cracks.* Journal of Applied Mechanics Vol. 35, pp. 379-386, 1968

[20] D. Roylance, *Introduction to Fracture Mechanics.* 2001

[21] I. Scheider, *Cohesive Model for Crack Propagation Analyses of Structures with Elastic-Plastic Material Behavior.* GKSS Research Center Geesthacht, 2001

[22] I. Scheider, W. Brocks, *The Effect of the Traction Separation Law on the Results of Cohesive Zone Crack Propagation Analyses*, 2003

[23] K-H. Schwalbe, A. Cornec, *Modelling Crack Growth Using Local Process Zones.* GKSS Research Centre Geesthacht, Germany, 1994

[24] T. Siegmund, W. Brocks *A Numerical Study on the Correlation Between the Work of Separation and the Dissipation Rate in Ductile Fracture.* 2000

[25] T. Siegmund, W. Brocks, *The Role of Cohesive Strength and Separation Energy for Modeling of Ductile Fracture. Fatigue and Fracture Mechanics: 30th Volume*, 2000, pp. 139-151.

[26] B. Sundström and other writers, *Handbok och Formelsamling i Hållfasthetslära.* Institutionen för hållfasthetslära KTH, 1998

[27] V. Tvergaard, J.W. Hutchinson, *The Relation Between Crack Growth Resistance and Fracture Process Parameters in Elastic-Plastic Solids.* 1992

[28] D. Xie, A.M. Waas, *Discrete Cohesive Zone Model for Mixed-Mode Fracture Using Finite Element Analysis.* Department of Aerospace Engineering, The University of Michigan, 2006

[29] A. Yavari, *Generalization of Barenblatt's Cohesive Fracture Theory for Fractal Cracks.* California Institute of Technology, 2001

[30] *Abaqus Analysis, User's Manual: Volume IV.* Dassault Systèmes, 2011

13 References - Images

[1] Date that collected: 2014-12-09
`http://upload.wikimedia.org/wikipedia/commons/thumb/e/e7/Fracture_modes_v2.svg/2000px-Fracture_modes_v2.svg.png`

[2] Image from figure 2.1 in
T.L. Andersson, *Fracture Mechanics - Fundamentals and Applications*. Department of Mechanical Engineering, Texas A&M University. CRC Press, 1991.

[3] Image from figure 7a in
J.R. Rice, *A Path Independent Integral and the Approximate Analysis of Strain Concentration by Notches and Cracks*. Journal of Applied Mechanics Vol. 35, pp. 379-386, 1968

[4] Image from figure 1.1 in
I. Scheider, *Cohesive Model for Crack Propagation Analyses of Structures with Elastic-Plastic Material Behavior*. GKSS Research Center Geesthacht, 2001

[5] Image from figure 3b in
A. Yavari, *Generalization of Barenblatt's Cohesive Fracture Theory for Fractal Cracks*. California Institute of Technology, 2001

[6] Image from figure 31.5.6-1 in
Abaqus Analysis, User's Manual: Volume IV. Dassault Systèmes, 2011

[7] Image from figure 31.5.6-5 in
Abaqus Analysis, User's Manual: Volume IV. Dassault Systèmes, 2011

[8] Image from figure 1 in
V. Tvergaard, J.W. Hutchinson, *The Relation Between Crack Growth Resistance and Fracture Process Parameters in Elastic-Plastic Solids*. 1992

[9] Image from figure 1 in
A. Needleman, *A Continuum Model for Void Nucleation by Inclusion Debonding*. Division of Engineering, Brown University, 1987

[10] Image from figure 2 in
A. Cornec, I. Scheider, K-H. Schwalbe, *On the Practical Application of the Cohesive Model*. Institute for Materials REsearch, GKSS Research Centre Geesthacht, 2003

[11] Image from figure 2 in
K-H. Schwalbe, A. Cornec, *Modelling Crack Growth Using Local Process Zones*. GKSS Research Centre Geesthacht, Germany, 1994

[12] Image from figure 3b in
K-H. Schwalbe, A. Cornec, *Modelling Crack Growth Using Local Process Zones*. GKSS Research Centre Geesthacht, Germany, 1994

[13] Image from figure 31.5.3-2 in
Abaqus Analysis, User's Manual: Volume IV. Dassault Systèmes, 2011